Title

Susceptibility-weighted MR imaging of radiation therapy-induced cerebral microbleeds in patients with glioma: a comparison between 3T and 7T

Journal

Neuroradiology, 56(2)

ISSN

0028-3940

Authors

Bian, Wei
Hess, Christopher P
Chang, Susan M
et al.

Publication Date

2014-02-01

DOI

10.1007/s00234-013-1297-8

Peer reviewed

HHS Public Access

Author manuscript

Neuroradiology. Author manuscript; available in PMC 2016 July 12.

Published in final edited form as:

Neuroradiology. 2014 February ; 56(2): 91–96. doi:10.1007/s00234-013-1297-8.

Susceptibility-weighted MR Imaging of Radiation Therapy-induced Cerebral Microbleeds in Patients with Glioma: A Comparison Between 3T and 7T

Wei Bian[1,2], **Christopher P. Hess**[2], **Susan M. Chang**[3], **Sarah J. Nelson**[1,2,4], and **Janine M. Lupo**[2]

[1]The UC Berkeley & UCSF Graduate Program in Bioengineering, University of California San Francisco, San Francisco, CA, USA

[2]Department of Radiology and Biomedical Imaging, University of California San Francisco, San Francisco, CA, USA

[3]Department of Neurological Surgery, University of California San Francisco, San Francisco, CA, USA

[4]Department of Bioengineeing and Therapeutic Sciences, University of California San Francisco, San Francisco, CA, USA

Abstract

Introduction—Cerebral microbleeds have been observed in normal-appearing brain tissue of patients with glioma years after receiving radiation therapy. The contrast of these paramagnetic lesions varies with field strength due to differences in the effects of susceptibility. The purpose of this study was to compare 3T and 7T MRI as platforms for detecting cerebral microbleeds in patients treated with radiotherapy using SWI.

Methods—SWI was performed with both 3T and 7T MR scanners on 10 patients with glioma who had received prior radiotherapy. Imaging sequences were optimized to obtain data within a clinically acceptable scan time. Both T2*-weighted magnitude images and SWI data were reconstructed, minimum-intensity projection was implemented, and microbleeds were manually identified. The number of microbleeds was counted and compared among datasets.

Results—Significantly more microbleeds were identified on SWI than magnitude images at both 7T (p=0.002) and 3T (p=0.023). 7T SWI detected significantly more microbleeds than 3T SWI for 7 out of 10 patients who had tumors located remote from deep brain regions (p=0.016), but when the additional 3 patients with more inferior tumors were included, the difference was not significant.

Address correspondence to: Janine M. Lupo, 1700 4th Street, UCSF Campus Box 2532, Byers Hall Room 303, San Francisco, CA 94158, Phone: 1-415-502-0646, Fax: 1-415-514-1028, janine.lupo@ucsf.edu.

This study was presented in part at the 20th annual meeting of the International Society for Magnetic Resonance in Medicine, 2012, Melbourne, Australia.

Conflict of interest

Grant support for this project was funded in part by GE Healthcare.

Conclusion—SWI is more sensitive for detecting microbleeds than magnitude images at both 3T and 7T. For areas without heightened susceptibility artifacts, 7T SWI is more sensitive to detecting radiation therapy-induced microbleeds than 3T SWI. Tumor location should be considered in conjunction with field strength when selecting the most appropriate strategy for imaging microbleeds.

Keywords

Cerebral microbleeds; Radiation therapy; Susceptibility-weighted imaging; 7T

Introduction

Gliomas are the second most common type of primary brain tumors with heterogeneous and diffuse histopathology. Radiation therapy is a mainstay their treatment with the goal of removing as much residual tumor as possible following maximal safe surgical resection. However, even with modern technology and treatment planning strategies, radiation therapy can cause injury to normal brain tissue [1]. One of the principal effects of radiation injury is cerebral hemorrhage, which over time results in the formation of cerebral microbleeds (CMBs) that comprise focal perivascular collections of hemosiderin and persist for years after receiving treatment [2, 3].

Since hemosiderin is a paramagnetic ferric-containing protein and its susceptibility effect results in local dephasing and subsequent loss of signal, CMBs are manifested as small, round, hypointense lesions on T2*-weighted images obtained using gradient echo sequences. The clinical relevance of detecting CMBs in cerebrovascular disorders such as cerebral amyloid angiopathy and hypertensive encephalopathy has been widely discussed, but their role as a potential diagnostic and prognostic marker is still under debate [4–6]. While relatively few studies have addressed radiation therapy-induced CMBs in gliomas, we have recently found that these lesions are distinct from calcification, are not related to patient age, increase in number over time since irradiation, and correlate with the dose and the target volume defined for radiation therapy [2]. This indicates that their burden may be a useful measurement of parenchymal radiation injury and therefore provide information for treatment evaluation.

Although the susceptibility effect scales with field strength and MR magnitude images that were acquired from scanners with field strength of 3T or 7T have been reported to detect more CMBs compared to those from 1.5T [7, 8], it is not clear how much sensitivity is gained with 7T over 3T for CMB detection, which is often confounded by macroscopic susceptibility artifacts and/or iron-rich tissues. Susceptibility-weighted imaging (SWI) combines information from both magnitude and phase images from a T2*-weighted gradient echo sequence, further enhancing the susceptibility effect and thus improving the detection sensitivity of CMBs [7, 9, 10]; yet, there has been recent debate as to whether SWI is necessary at 7T where there is already heightened susceptibility in magnitude images. The purpose of this study was to compare 3T and 7T SWI and magnitude images for the detection of radiation therapy-induced CMBs in patients with treated gliomas and evaluate

how the presence of susceptibility-induced artifacts and altered contrast affect detection sensitivity at 7T.

Methods

Patients

Ten patients with glioma who received radiation therapy between 2 and 15 years prior to the date of imaging, were recruited for this study. All patients were scanned at both 3T and 7T field strengths on the same day. This varied population allowed for a wide range of CMB locations, contrasts, and sizes, thereby creating a broad spectrum of detection sensitivities from which to evaluate the different acquisition strategies. The study was approved by our Committee of Human Research and written informed consent was obtained from all subjects.

MR Imaging and Image Processing

High resolution T2*-weighted imaging with a 3D flow-compensated spoiled gradient echo sequence was performed using whole-body 3T and 7T scanners (GE Healthcare Technologies, Milwaukee, WI) with 8-channel phased array coils. The TE/TR was 28/56ms at 3T and 16/50ms at 7T. A GRAPPA-based parallel imaging acquisition was implemented with either a 2-fold (3T) or 3-fold (7T) acceleration factor and 16 autocalibrating lines to keep the total acquisition time within 7 minutes. A flip angle of 20°, 24cm FOV, and in-plane resolution of 0.5×0.5mm, and 2mm slice thickness were used for both field strengths [11].

The raw complex k-space data from all channels were transferred off-line to a SunBlade 2000 Workstation (Sun Microsystems, Santa Clara, CA) and post-processing was performed using in house programs developed with Matlab 7.1 software (MathWorks Inc., Natick, MA) on a Linux cluster running Sun's N1 Grid Engine. A GRAPPA-based reconstruction was utilized to restore the full complex k-space data of each individual coil before employing standard SWI processing [11]. Phase masks were constructed from the full complex k-space data of each individual coil element through complex division by a low-pass filtered image and scaling the resulting negative phase values between zero and one [12]. To generate a susceptibility-weighted image, the phase mask was then multiplied with the corresponding magnitude image from each channel 4 times, and the resulting images from each channel were combined by the square root of sum of squares method. A 72×72 Hanning low-pass filter was used for phase mask generation at 3T, while a larger filter size of 96×96 was used at 7T due to the higher frequency phase wraps present at 7T compared to 3T. A low pass filter with edge completion was applied to the combined images to minimize any residual intensity variation across the image. Finally, minimum intensity projection (mIP) images were generated through 8 mm-thick slabs of overlapping volumes between 3T and 7T images for both magnitude images and SWI in order to provide uniform coverage for analysis.

Microbleed Counting

Microbleeds were identified as small hypointense foci that did not correspond to vessels on consecutive slices, and counted in normal-appearing tissue outside the tumor region. Veins that traversed the axial image plane mimicking CMBs were excluded if they were of linear structure or skewed from the axis, as illustrated in Figure 1. CMBs were counted independently by two trained raters with 6 and 11 years experience in brain tumor imaging, taking into account that the same lesion could be conspicuous on adjacent slices. In ambiguous cases, both reviewers reached a consensus after discussion with a subspecialty certified neuroradiologist. To reduce recall bias, different image sets from a same patient were examined at least one week apart and in random order.

Statistical Analysis

A two-sample paired Wilcoxon signed-rank test was performed to test whether there was a significant difference in the number of CMBs between image sets. The significance level was set to an alpha of 0.05.

Results

A total of 208 CMBs (mean: 20.8; range: 10~42) were detected using 3T SWI and 159 (mean: 15.9; range: 9~31) on the corresponding magnitude images. The 7T SWI and magnitude images detected 236 (mean: 23.6; range: 13~43) and 153 (mean: 15.3; range: 7~30) CMBs, respectively. Table 1 shows the CMB count and tumor location for each patient, and the results of statistical comparisons between different image sets are listed in Table 2.

Image Processing: SWI vs. Magnitude

There was a significant difference at both field strengths (7T: $p = 0.002$; 3T: $p = 0.004$) in the number of CMBs seen on magnitude and SWI images, with 54.2% more CMBs detected at 7T and 30.8% more CMBs detected at 3T. The contrast of CMBs to surrounding brain tissue was also greatly improved on 7T SWI compared to magnitude images, as shown in Figure 2(a). When gain in the number of CMBs for SWI versus magnitude images was compared between 3T and 7T on a patient-by-patient basis, the gain was larger at the higher field strength ($p = 0.037$).

Field Strength: 7T vs. 3T

Seven (patients 1–7 in Table 1) of 10 patients had more CMBs identified on 7T SWI. The other 3 patients (patients 8–10 in Table 1), who had more CMBs detected at 3T, had tumors in the temporal lobe or basal ganglia. When all 10 patients were considered, there was no significant difference in the number of CMBs detected at the two field strengths. However, when the 3 patients with tumors in the temporal lobe or basal ganglia were excluded the difference was significant ($p = 0.016$). A representative example is shown in Figure 3 (a and b), where (a) shows heightened CMB contrast at 7T SWI compared to 3T SWI and (b) shows CMBs masked by susceptibility artifacts at 7T SWI. Of the CMBs detected by SWI, 112 were seen at 7T but not identified at 3T, while 84 were seen at 3T but not identified at 7T. There was no difference in CMB detection between 7T and 3T magnitude images, even

after removing the latter 3 patients. In addition, 3T SWI detected significantly more CMBs than 7T magnitude images ($p = 0.023$), as shown in Figure 2(b).

Discussion

The results of this study demonstrate that detection of radiation therapy-induced CMBs benefits from applying SWI at 7T in two ways. First, 7T SWI images detected more CMBs compared to magnitude images from the same field strength. This is consistent with observations from previous studies [7, 10]. Second, 7T magnitude images were less sensitive in detecting CMB than 3T SWI images. Note that the incremental gain in sensitivity achieved by using SWI was even larger at 7T compared to 3T, probably because of the increased SNR and susceptibility contrast on phase images from the former.

Although 3T and 7T SWI showed no significant difference in CMB detection for the entire patient group, there were significantly more CMBs detected at 7T for the seven patients (patients 1–7 in Table 1) who had tumors located remotely from deep brain structures. The improved sensitivity of 7T SWI to CMBs in this subgroup of patients may help early diagnosis of radiation-induced microvascular injury [2, 3]. Initial studies have shown that the number of CMBs increases over time since receiving radiation therapy and often extend well beyond the initial high-dose volume and into the contralateral hemisphere as time progresses [2]. Although the exact role of CMBs remains to be seen, they have been implicated as prognostic markers of neurocognitive impairment in other diseases such as TBI, CAA, stroke, mild cognitive impairment and Alzheimer's disease [13–19]. Thus, earlier detection of them using ultra-high field scanners (7T and above) may be beneficial in the clinic for patient management and prevention of further cognitive decline. This may be especially relevant for designing future treatment strategies for patients with low-grade gliomas, who have longer progression-free survival compared to more aggressive high-grade tumors, where there is debate as to whether the benefits of radiotherapy outweigh the potential negative effects [20].

The decreased CMB detection sensitivity at 7T for the remaining three patients (patients 8~10 in Table 1) was mostly due to macroscopic susceptibility artifacts often located near air-tissue interfaces that result in residual phase wrapping that is difficult to eliminate with standard SWI filtering methods (see the bottom row in Figure 3(b)), as the filter size must be selected to balance heightened phase contrast with removal of residual high frequency phase wraps. Enhanced susceptibility of iron-rich tissues such as the basal ganglia (see the top row in Figure 3(b)) also can obscure CMBs at 7T. Although in this study we used standard SWI processing that would be routinely available in the clinic for comparison purposes, more advanced post-processing and local field correction algorithms [21, 22] should be applied to mitigate these artifacts and recover the missed CMBs at 7T.

Previous studies are consistent with higher field strength and SWI providing improvements in detecting CMBs [7, 10]. Nandigam *et al.* [10] compared CMB detection between 3T and 1.5T and found that SWI images detected significantly more CMBs at 3T. The population considered in that study was patients with cerebral amyloid angiopathy, for whom the characteristic superior location of CMBs made them less likely to be obscured by

susceptibility artifacts. Another comparison study between 7T and 1.5T SWI performed by Theysohn *et al.* [7] found an improved sensitivity of CMB detection at 7T for patients with vascular dementia, where all CMBs that were visible at 1.5T were also detected at 7T. This result was not surprising given that these microbleeds were relatively large and of high contrast in order to be detected at 1.5T. In our comparison between 3T and 7T, 40.4% of CMBs that were observed on 3T SWI were not visible on 7T SWI. Our results suggest that the increase in susceptibility contrast may be offset by there being more artifacts at 7T relative to 3T, and is further supported by the observation that there was no difference in CMB detection for magnitude images between 3T and 7T.

Knowing that macroscopic susceptibility artifacts can degrade the sensitivity of detecting CMBs is important for selecting methods for imaging glioma patients who have received radiation therapy. This may also be true in hypertensive arteriopathy, where CMBs are located primarily in deep brain [4]. 7T SWI would be preferred over 3T SWI as long as the tumor location is away from deep brain, because the heightened contrast may be especially critical in visualizing small CMBs or following them as they evolve over time. A better understanding of the evolution of CMBs would help in the exploration of their relationship to microvasculature damage and prognostic values.

The limitations of this study are similar to those that have been reported in previous studies. [7, 8, 10] Since sequence timing parameters must be altered between field strengths, the selection of these parameters can also affect CMB detection. However, since we individually optimized both imaging acquisitions and post-processing steps for CMB detection at each field strength with similar scan times, the degree of bias should be minimized. Another limitation was that the angle of obliquity of the image acquisition was not necessarily identical between 3T and 7T, even though care was taken during prescription to cover the same region. Although performing a minimum intensity projection through 8mm of tissue helps mitigate any discrepancy due to this variation in head position, we were also careful to search adjacent slices for microbleeds that were not visible on all sets of images. Overall, differences in coverage between field strengths were minimal and our analysis was restricted to the joint FOV of both acquisitions.

Conclusions

In conclusion, our study confirms that 7T SWI is more sensitive to radiation therapy-induced CMBs than SWI at 3T, as long as the location of CMBs is not in areas with heightened susceptibility artifacts. Tumor location should be considered in conjunction with field strength when designing protocols for detecting radiation therapy-induced CMBs in patients with glioma. The gain in sensitivity due to SWI processing is significant for detecting CMBs at both 3T and 7T.

Acknowledgments

The authors would like to thank Andre Cote, Adam Elkhaled, Angela Jakary and Trey Jalbert for their work in MR image acquisition and Bert Jimenez and Mary McPolin for their clinical coordination of patient MR scans. This work was supported by UC Discovery grant ITL-BIO04-10148, which is an academic-industry partnership grant with General Electric Healthcare, a UCSF REAC Cohn & Simon Memorial Fund, and a fellowship from the

Graduate Education in Medical Sciences (GEMS) training program funded by Howard Hughes Medical Institute (HHMI).

References

1. Valk PE, Dillon WP. Radiation-Injury of the Brain. American Journal of Neuroradiology. 1991; 12(1):45–62. [PubMed: 7502957]
2. Lupo JM, et al. 7-Tesla susceptibility-weighted imaging to assess the effects of radiotherapy on normal-appearing brain in patients with glioma. Int J Radiat Oncol Biol Phys. 2012; 82(3):e493–500. [PubMed: 22000750]
3. Shobha N, Smith EE, Demchuk AM, Weir NU. Small vessel infarcts and microbleeds associated with radiation exposure. Can J Neurol Sci. 2009 May; 36(3):376–8. [PubMed: 19534343]
4. Charidimou A, Werring DJ. Cerebral microbleeds: detection, mechanisms and clinical challenges. Future Neurol. 2011; 6(5):587–611.
5. Greenberg SM, et al. Cerebral microbleeds: a guide to detection and interpretation. Lancet Neurology. 2009; 8(2):165–174. [PubMed: 19161908]
6. Cordonnier C, Al-Shahi Salman R, Wardlaw J. Spontaneous brain microbleeds: systematic review, subgroup analyses and standards for study design and reporting. Brain. 2007; 130(Pt 8):1988–2003. [PubMed: 17322562]
7. Theysohn JM, et al. 7 Tesla MRI of Microbleeds and White Matter Lesions as Seen in Vascular Dementia. Journal of Magnetic Resonance Imaging. 2011; 33(4):782–791. [PubMed: 21448941]
8. Conijn MM, et al. Cerebral microbleeds on MR imaging: comparison between 1.5 and 7T. AJNR Am J Neuroradiol. 2011; 32(6):1043–9. [PubMed: 21546463]
9. Ayaz M, et al. Imaging Cerebral Microbleeds Using Susceptibility Weighted Imaging: One Step Toward Detecting Vascular Dementia. Journal of Magnetic Resonance Imaging. 2010; 31(1):142–148. [PubMed: 20027582]
10. Nandigam RNK, et al. MR Imaging Detection of Cerebral Microbleeds: Effect of Susceptibility-Weighted Imaging, Section Thickness, and Field Strength. American Journal of Neuroradiology. 2009; 30(2):338–343. [PubMed: 19001544]
11. Lupo JM, et al. GRAPPA-based susceptibility-weighted imaging of normal volunteers and patients with brain tumor at 7 T. Magn Reson Imaging. 2009; 27(4):480–8. [PubMed: 18823730]
12. Haacke EM, et al. Susceptibility weighted imaging (SWI). Magnetic Resonance in Medicine. 2004; 52(3):612–618. [PubMed: 15334582]
13. Charidimou A, Krishnan A, Werring DJ, Rolf Jäger H. Cerebral microbleeds: a guide to detection and clinical relevance in different disease settings. Neuroradiology. 2013 Jun; 55(6):655–74. Epub 2013 May 25. [PubMed: 23708941]
14. Ayaz M, Boikov AS, Haacke EM, Kido DK, Kirsch WM. Imaging cerebral microbleeds using susceptibility weighted imaging: one step toward detecting vascular dementia. J Magn Reson Imaging. 2010 Jan; 31(1):142–8. [PubMed: 20027582]
15. van Norden AG, van den Berg HA, de Laat KF, Gons RA, van Dijk EJ, de Leeuw FE. Frontal and Temporal Microbleeds Are Related to Cognitive Function: The Radboud University Nijmegen Diffusion Tensor and Magnetic Resonance Cohort (RUN DMC) Study. Stroke. 2011 Sep 22. Epub ahead of print.
16. Werring DJ, Gregoire SM, Cipolotti L. Cerebral microbleeds and vascular cognitive impairment. J Neurol Sci. 2010; 299:131–135. [PubMed: 20850134]
17. Goos JD, Kester MI, Barkhof F, et al. Patients with Alzheimer disease with multiple microbleeds: relation with cerebrospinal fluid biomarkers and cognition. Stroke. 2009; 40:3455–3460. [PubMed: 19762705]
18. Kinnunen KM, Greenwood R, Powell JH, Leech R, Hawkins PC, Bonnelle V, Patel MC, Counsell SJ, Sharp DJ. White matter damage and cognitive impairment after traumatic brain injury. Brain. 2011 Feb; 134(Pt 2):449–63. Epub 2010 Dec 29. [PubMed: 21193486]
19. Scheid R, Preul C, Gruber O, Wiggins C, von Cramon DY. Diffuse axonal injury associated with chronic traumatic brain injury: evidence from T2*-weighted gradient-echo imaging at 3 T. AJNR Am J Neuroradiol. 2003 Jun-Jul;24(6):1049–56. [PubMed: 12812926]

20. Shaw EG. Low-grade gliomas: to treat or not to treat? A radiation oncologist's viewpoint. Arch Neurol. 1990; 47(10):1138–40. [PubMed: 2222248]

21. Jin Z, Xia L, Du YP. Reduction of artifacts in susceptibility-weighted MR venography of the brain. Journal of Magnetic Resonance Imaging. 2008; 28(2):327–33. [PubMed: 18666154]

22. Liu T, et al. Cerebral microbleeds: burden assessment by using quantitative susceptibility mapping. Radiology. 2012; 262(1):269–78. [PubMed: 22056688]

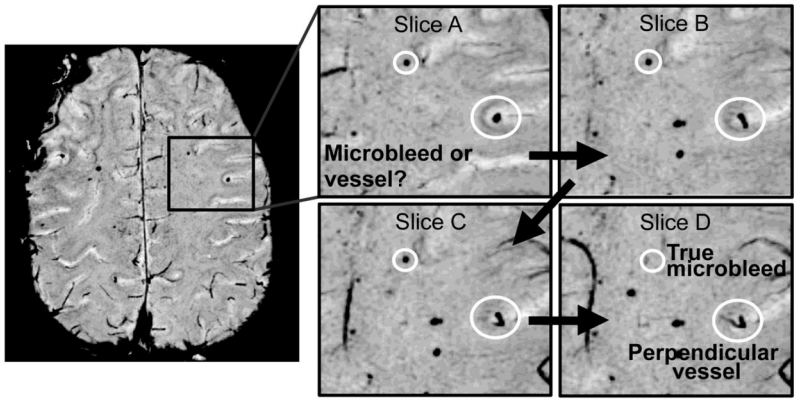

Fig 1.

Illustration of how CMBs were identified as foci of susceptibility that excluded vessels, tumor, or surgical borders on consecutive slices.

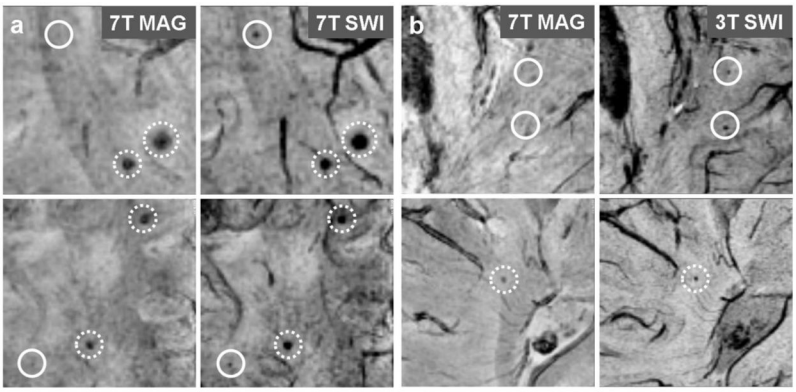

Fig 2.

(a) 7T magnitude and SWI images from patient 7 (*top row*) and 10 (*bottom row*). *Solid circle*: CMBs seen on 7T SWI only; *Dashed circle*: CMBs better contrasted on 7T SWI compared to 7T magnitude images. (b) 3T SWI and 7T magnitude images from patient 3 (*top row*) and 2 (*bottom row*). Solid circle: CMBs seen on 3T SWI only; Dashed circle: CMBs better contrasted on 3T SWI compared to 7T magnitude images.

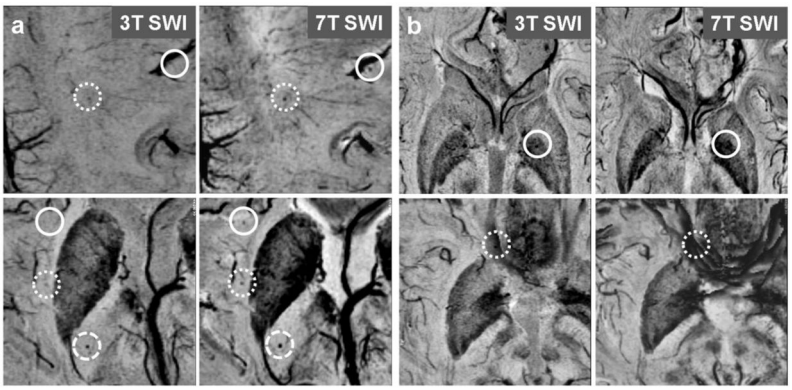

Fig 3.

(a) 3T (*left column*) and 7T (*right column*) SWI images from patient 2 (*top row*) and 3 (*bottom row*). *Solid circle*: CMBs seen on 7T SWI only; *Densely-dashed circle*: CMBs better contrasted on 7T SWI compared to 3T SWI; *Loosely-dashed circle*: CMBs seen on both 7T and 3T SWI. (b) 3T and 7T SWI images from patient 8 (top row) and 3 (bottom row). *Solid circle*: CMBs seen on 3T SWI but masked by the enhanced susceptibility effect of iron within the globus pallidus on 7T SWI; *Dashed circle*: CMBs seen on 3T SWI but masked by the phase wrap artifacts on 7T SWI.

Table 1

CMB Counts from 10 Patients on 3T and 7T images

Patients	3T				7T				Tumor Location
	Magnitude	SWI-all	SWI-3T only	Gain with SWI (%)	Magnitude	SWI-all	SWI-7T only	Gain with SWI (%)	
1	10	12	6	20.0	11	16	10	45.5	Frontal Lobe
2	9	10	5	11.1	11	13	8	18.2	Frontal Lobe
3	11	18	2	63.6	15	28	12	86.7	Frontal Lobe
4	11	13	5	18.2	11	18	10	63.6	Frontal Lobe
5	13	18	7	29.0	18	30	10	43.3	Parietal Lobe
6	31	40	10	38.5	30	43	22	66.7	Cerebellum/Brain stem
7	21	23	6	9.5	23	31	14	34.8	Cerebellum/Brain stem
8	18	18	8	0.0	7	15	5	114.3	Frontal Lobe/Basal Ganglia
9	13	14	10	7.7	8	13	9	62.5	Frontal Lobe/ Basal Ganglia
10	22	42	25	90.9	19	29	12	52.6	Temporal Lobe
Total	**159**	**208**	**84**	**30.8**	**153**	**236**	**112**	**54.2**	

Table 2

Significant Differences in CMB Detection between Different Image Sets

	Comparison Groups	*p* Value (N=10)	*p* Value (N=7)*
Field Strength	**SWI:** *3T vs. 7T*	0.193	**0.016**
	SWI: *only at 3T vs. only at 7T*	0.193	**0.016**
	Magnitude: *3T vs. 7T*	0.984	0.094
	3T SWI vs. 7T Magnitude	**0.023**	--
	% Gain with SWI: *3T vs. 7T*	**0.037**	--
Image Processing	**3T:** *SWI vs. Magnitude*	**0.004**	--
	7T: *SWI vs. Magnitude*	**0.002**	--

*Excluding the last 3 patients in Table 1, who had tumors located in deep brain tissue.

P-values in bold are significant